

Distortion of surfactant lamellar phases induced by surface roughness

Shirin Nouhi^{1*}, Alexandros Koutsioubas², Vassilios Kapaklis¹ and Adrian R. Rennie¹

1. Centre for Neutron Scattering, Uppsala University, Box 516, 75120, Uppsala, Sweden
2. Jülich Centre for Neutron Science (JCNS) at Heinz Maier-Leibnitz Zentrum (MLZ), Forschungszentrum Jülich GmbH, Lichtenbergstr. 1, 85748 Garching, Germany

* Corresponding author, E-mail address: shirin.nouhi@physics.uu.se

Abstract

Self-assembly is a characteristic property of soft matter and understanding the factors which assist or perturb this process is of a great importance in many biological and industrial processes. Amphiphiles self-assemble and order into a variety of structures including well-ordered lamellar phases. The present work uses neutron reflectometry to explore the effects of both interface roughness and temperature on the lamellar-phase structure of a non-ionic surfactant at a solid/liquid interface. The structure of concentrated solutions of tetraethyleneglycol dodecyl ether has been compared against a smooth surface and one with a roughness of the order of the lamellar spacing. The results showed that the surfactant forms a well-order and aligned structure at smooth surface that extends to a depth of micrometers from the interface. Increasing the temperature of the sample and subsequent cooling helped the alignment and increased the number of oriented layers at the surface. The same sample formed a significantly less aligned structure at a rough surface that did not align to same extent after heating. The perturbation of the structure caused by thermal fluctuations was found to be much less than that imposed by a small surface roughness.

Keywords

Roughness, thermal fluctuations, disorder, neutron reflectometry, nonionic surfactant

Introduction

Amphiphiles with hydrophilic head groups and hydrophobic hydrocarbon tail regions occur widely as detergents, in biological membranes and in formulations for personal care and pharmaceutical products, coatings, etc. [1-4]. They self-assemble and order into a variety of structures such as micelles, liquid crystal phases, microemulsions and other structures that display both long-range order and interesting dynamics. At solid/liquid interfaces, amphiphiles can organize themselves into well-ordered bilayer and even as multilayer structures. The structure and ordering of molecules at an interface is strongly influenced by both the physical and chemical properties [5, 6]. Often simple ideas of the relative volumes of hydrophilic ‘head’ groups and hydrophobic ‘tails’ are used as guides to how surfactants will pack as planar or curved aggregates [7, 8]. The induced ordering of amphiphiles by surfaces and interfaces has been discussed previously from both theoretical [9, 10] and experimental perspectives [11, 12], and this was found to be a key factor in determining their behavior and use in many potential applications [13]. For example, ordering in liquid crystal structures plays an important role in the biological function of cells, and disorder or defects can increase the risk of for example tissue cancer [14, 15].

There is considerable similarity between diblock copolymers and surfactants in that they both consist of two moieties that may tend to phase separate and can have quite different interactions with solvent molecules. Nanolithographic methods have been shown to direct self-assembly of diblock copolymers in terms of orientation and positional ordering [16, 17]. In particular molecules with ethylene oxide head groups and alkyl tails that are often written as C_nEO_m where n is the number of carbons in the tail and m is the number of ethylene oxide groups are like very short copolymers. The structure formed by amphiphiles can be perturbed by temperature, physical and chemical properties of surfaces, and the addition of other components such as solvent. Understanding these different factors that induce or disturb the order of amphiphiles at interfaces is a major challenge, especially distinguishing between the effects when several perturbations are combined. Changes due to the addition of a new component such as spherical particles to the lamellar phase of $C_{12}EO_5$ have been described by Imai et al. and shown to influence the interlamellar interactions by imposing geometrical constraints on the packing of a

planar structure [18-20]. The addition of colloidal particles suppressed the lamellar fluctuations, even at very low concentrations below 1 vol.%, and caused the lamellar structures to change to micelles at higher concentrations above ~ 3 vol.%.

There have been various previous investigations of textured surfaces. It has been shown that lipid bilayers can assemble onto arrays of nanowires, of typically 100 nm diameter and length of a few μm following the topology of the nanowires over millimeter-sized areas [21]. Surfactant adsorption on surfaces with different roughness has been shown to occur with different kinetics and to equilibrate at different final amounts [22]. They found that the initial rate of adsorption for hexadecyl trimethyl ammonium bromide (CTAB), both below and above its critical micelle concentration, was higher on a rough surface, although the adsorption completed faster on the smooth surfaces. The structure of adsorbed CTAB was observed to be different on rough and smooth surfaces [23] with thicker and asymmetric bilayers that have a lower packing density and surface coverage formed on a rough surface.

In the case of surfactant multilayers, a balance between the interactions in the bulk, those arising from stacking layers and with the solid surface determines the structure of lamellae. In the present study, we explore the influence of surface roughness on multilayer structures to gain understanding of the extent that small geometric perturbations, with length scales approximately the same as the lamellar spacing, influence the long-range ordering of surfactants. For this purpose, we have chosen a non-ionic surfactant, with known properties, as a model system in a concentration range, where ordered multilayer structures can form. The structure of the surfactant is studied against a smooth and a rough surface at different temperatures, so that the effect of surface roughness can be distinguished from the perturbation due to thermal fluctuations.

Materials

In the present study, we used the non-ionic surfactant Brij L4, which has an average formula $C_{12}H_{25}(OCH_2CH_2)_4OH$ (tetraethylene glycol dodecyl ether), or $C_{12}EO_4$, although there is some distribution of number of ethylene oxide moieties, (Sigma Aldrich, P4391) and was diluted in water to concentrations of 40 and 55 vol.%. The sample at the higher concentration was very viscous and was stirred using a glass rod for about two minutes to

make certain it was uniformly mixed. Previous studies reported the phase diagram of $C_{12}EO_4$ in H_2O [24] and the phase diagram of shorter ($C_{12}EO_3$) or longer ($C_{12}EO_5$) surfactants [25, 26]. Figure S1, in the supporting information, shows the phase diagram for $C_{12}EO_4$ in H_2O from Mitchell et al., 1983 with the region measured marked on this study marked in red. The exact phase boundaries that have been reported, with respect to temperature and concentration, differ slightly. However, they all agree that both 40 and 55 vol.% Brij L4 is in the lamellar phase for the temperature range measured in this experiment.

Silicon crystals $5\text{ cm} \times 5\text{ cm} \times 1\text{ cm}$ cut with (111) planes on the large face were purchased from Crystran. One of the crystals was used with the polished smooth surface and the other crystal was etched and roughened in basic solution (pure Decon90) for 24 hours. The roughness of the crystals was then checked with atomic force microscopy (see Figure S2a, supporting information) and X-ray reflectivity measurements. Neutron reflectivity data (explained below) from the clean surface before injecting the samples are shown in Figure S2b, in supporting information. Both crystals were cleaned as described in our previous studies (see reference 27 for details). The cleaned crystals were characterized using neutron reflectivity with D_2O , H_2O and a mixture of water that is neutron refractive index matched to silicon in order to determine the thickness of the oxide layer and roughness of the surface, in-situ prior to the sample injection. The smooth crystal surface was found to have an oxide (SiO_2) layer that was $\sim 10\text{ \AA}$ thick and with a roughness of $\sim 3\text{ \AA}$. The rough crystal was found to have a porous oxide layer with about 20 % water in a layer of 60 \AA thickness with roughness of $\sim 30\text{ \AA}$.

Methods and experimental set-up

Neutrons have a high penetration depth into some materials such as silicon which makes them a useful tool to study the structures at solid/liquid or so-called buried interfaces. Neutrons are transmitted, refracted or reflected when at an interface. The interfaces relevant for neutrons are the boundaries between layers with different scattering length density. The scattering length density, ρ , of a material is given by:

$$\rho = \sum n_i b_i \quad (1)$$

where n_i is the number density for atoms of element i , and b_i is the scattering length. The scattering length represents the interaction potential of each

element with neutrons and varies between different elements and isotopes. For example, neutrons have very different scattering length densities for H_2O and D_2O , see Table I for the values. Neutron reflectometry thus benefits from using H_2O , D_2O or a mixture of H_2O and D_2O to change the contrast and enhance the signal from particular components. The refractive index, n_r , for neutrons for a material is calculated from the scattering length density and wavelength, λ , as $n_r = 1 - (\lambda^2 \rho / 2\pi)$.

In this study, neutron reflectometry was used to investigate the structure of the Brij L4 lamellar phase and the ordering of the lamellar structure close to rough and smooth surfaces. The reflectivity, $R(\mathbf{Q})$ is the ratio between the intensity of the reflected and incident beams at the specular condition, $\theta_i = \theta_f$, where θ_i is the angle of the incident beam and θ_f is the angle of the outgoing beam. At the specular condition, the momentum transfer \mathbf{Q} is perpendicular to the interface, and the recorded signal provides information about the thickness, composition, and roughness of layers parallel to the interface. Reflectivity data is commonly shown against the magnitude of \mathbf{Q} perpendicular to the interface and is given by:

$$Q = (4\pi/\lambda) \sin(\theta_i) \quad (2)$$

where λ is the wavelength of the neutrons.

Neutron reflection experiments were performed on the MARIA reflectometer at MLZ, Munich [28, 29], which operates using a monochromatic beam and a vertical sample orientation. The resolution of MARIA is determined primarily by its 10 % spread of wavelength. Reflectivity data were collected with two different wavelengths, having a small overlapping region. Reflectivity data for $Q < 0.042\text{ \AA}^{-1}$ were collected with $\lambda = 10\text{ \AA}$ and in the range $0.035\text{ \AA}^{-1} < Q < 0.45\text{ \AA}^{-1}$ with $\lambda = 5\text{ \AA}$.

Data reduction: The scattered neutron signal on MARIA, is counted using a two-dimensional position sensitive detector, that allows the signal from both the specular reflection and the off-specular scattering to be recorded simultaneously. As described later, this allows interesting comparisons of interface and bulk structure, but it causes some challenges in the data reduction. Measurements consisted of coupled scans of the sample and detector, set in such way that the center of the detector meets the specular condition. Reflectivity values are obtained fitting a Gaussian peak at the center of the detector and additionally allowing for the background. However, for a strongly scattering sample such as our system, the

Bragg diffraction peaks from the bulk, which can fall on either side of the region of interest of the detector for evaluation of the intensity of specular reflection depending on the sample alignment, contribute significantly to the background. Hence estimating the absolute reflectivity and subtracting the signal on the sides of the intense Bragg peaks becomes challenging (see Figure S3, supporting information as an example). The effect becomes more pronounced when the Bragg peak is wider or there is more diffuse scattering due to random alignment in the surfactant structure. This effect is more pronounced at low Q ($< 0.05 \text{ \AA}^{-1}$) because of the relative magnitude of the different peaks, not allowing reliable discrimination of the various component. Hence, this region has been excluded from fitting of reflectivity.

Interpretation of reflectivity data

The reflectivity for a particular scattering length density profile can be calculated using the optical matrix method of Abelès [30]. Reflectivity data for the Brij lamellar structures were modelled using the *byban* program available on the web [31] which has been described also by Hellsing et al., 2011 [32]. The program allows the model to be constrained by imposing stoichiometry for the head and tail groups of the surfactant molecule. The structural parameters used for modelling the reflectivity profile in this study were the thickness of the head, t_h , and tail, t_t , region of surfactant, the area per molecule, A , the interlayer distance occupied by solvent, t_s , lamellar displacement due to thermal fluctuation, ζ , and the number of layers, N . The slight difference between the present model and Hellsing et al. 2011 is that we treated the bilayer as a four-layer structure (see figure 1), whereas Hellsing et al. 2011 have assumed the bilayer as a two-layer structure: one layer of surfactant (including both

heads and tails) and a solvent layer. We also had to vary the number of layers to compensate for the strong scattering for some reflectivity curves. The number of layers in this program is an integer which was manually adjusted until the model could fit the intensity of the at least the first Bragg peak which was highly influenced by this parameter. Figure 1 shows a schematic diagram of the first few layers of the lamellar structure and the corresponding scattering length density profile calculated for 55 vol.% Brij L4 at the Si/SiO₂/D₂O interface. The total bilayer thickness, d , is calculated as:

$$d = 2t_h + t_t \quad (3)$$

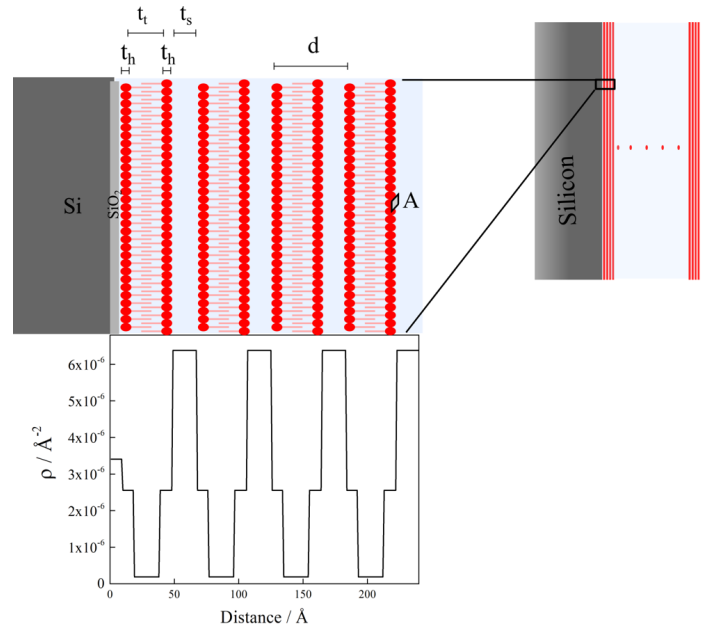


FIG 1. Scattering length density profile of the lamellar structure supported on a silica surface. t_h refers to the thickness of the head group, t_t to the thickness of tail group, t_s to thickness of solvent layer, A is the area per molecule and d to the total bilayer thickness.

TABLE I. Parameters used for modeling multilayer structure.

| Name | Formula | Formula Mass / g mol^{-1} | Density / g cm^{-3} | Molecular or formula volume / \AA^3 | Scattering length Σb / fm | ρ / 10^{-6} \AA^{-2} |
|------------------------|---|------------------------------------|------------------------------|--|-----------------------------------|-------------------------------------|
| Heavy water | D ₂ O | 20.03 | 1.105 | 30.0 | 19.1 | 6.35 |
| Water | H ₂ O | 18.02 | 0.9975 | 30.0 | -1.7 | -0.56 |
| Silicon | Si | 28.08 | 2.33 | 12.9 | 4.14 | 2.07 |
| Silicon oxide (silica) | SiO ₂ | 60.08 | 2.16 | 46.2 | 15.7 | 3.41 |
| Brij L4 | C ₁₂ H ₂₅ (OCH ₂ CH ₂) ₄ OH | 362.54 | 0.95 | 633.7 | 4.89 | 0.10 |
| Brij L4 tail | C ₁₂ H ₂₅ | 169.33 | 0.75 | 374.9 | -13.72 | -0.40 |
| Brij L4 head | (OCH ₂ CH ₂) ₄ OH | 170.33 | 0.99 | 258.8 | 18.62 | 0.70 |

The intensity and width of the observed peaks depends primarily on the scattering length density contrast and the number of the repeating layers. The width of the observed peak is also strongly influenced by the instrumental resolution. Our program allows convolution of the instrumental resolution in Q space with the model during the fitting process.

Lamellar structure is never perfect sheets of multilayer parallel to the surface. Long-range ordering of lamellar structure can be disturbed due to three main types of disorder which should be considered when modelling reflectivity data. These fluctuations can influence the relative intensity of the different order Bragg peaks and also broaden them. The first type of disorder occurs due to thermal fluctuations which cause the layers to fluctuate slightly around their mean position. This type of fluctuation is different to the intermixing or roughness of adjacent layers which can be included in models using the methods described by Névoit and Croce [33]. In the case of thermal fluctuations, the thickness and composition of different parts of the bilayer remain unchanged and a single bilayer fluctuates as a coherent unit (head and tail regions together) giving rise to local curvature of the layer. However, the fluctuation of different bilayers that are separated with a solvent layer, is not correlated and this decreases the intensity of the observed Bragg peaks. Thermal fluctuations can be in the same order of the lamellar spacing while roughness must be smaller than the thickness of layers and in the case of our model it is constrained to be a fraction of the thickness that is not allowed to exceed 0.3.

The scattered intensity, $I(Q)$, depends on the shape and size of inhomogeneities or differences in scattering length density, as well as the correlations between these differences. Thermal disorder also reduces the scattered intensity with an exponential dependence on the squared amplitude of the fluctuations, ξ [34, 35]:

$$I(Q) \propto \exp(-2w) \quad (4)$$

where $2w$ is known as the Debye-Waller factor that is defined as $Q^2\xi^2/3$. Disorder due to bending fluctuations is pronounced in the surfactant lamellar phases and can be related to the thermal fluctuations described by the Debye-Waller factor. These fluctuations for a membrane can be calculated from the Caillé parameter [36], η that depends on the bending modulus, K , and the compression modulus, B , of the lamellae and is given by:

$$\eta = \frac{\pi k_B T}{2d^2\sqrt{KB}} \quad (5)$$

k_B is Boltzmann's constant, T is the temperature, and d is the repeat distance of the bilayer [37].

This parameter can be related directly with the amplitude of the thermal fluctuations by:

$$\eta = \frac{\xi^2\pi^2}{d^2} \quad (6)$$

where ξ is the mean displacement from the central value [38]. These equations allow the mechanical response to be related to reflectivity and scattering data. In the present study, the mean displacement of the lamellae due to thermal fluctuations obtained from fitting reflectivity data was used to calculate the Caillé parameter and hence provide an estimate of the modulus.

A second type of disorder occurs due to small variations in the spacing of the layers and this decreases the intensity of the peaks very significantly. This type of disorder can be calculated for a structure with a variation in the lamellar spacing and this has been shown to decrease the intensity of Bragg peaks significantly. The reflectivity data measured for the samples in the present study show strong Bragg peaks including higher order diffraction and so the effect of this type of disorder is likely to be insignificant.

For a perfect lamellar structure Bragg peaks with equal spacing appear. The intensity of the peaks depends on the contrast and number of bilayers and the width of the peaks depends on the crystal size (number of layers) and the instrumental resolution. When the Bragg peaks are observed at the specular condition diffraction arises from crystal planes aligned parallel to the surface. The width provides information about the overall thickness of the aligned material at the surface. When diffraction is observed at other orientations, it probes a depth that is limited by the overall attenuation of the beam in the sample and corresponds to about 0.1 mm, thus effectively the bulk of the sample is observed. The crystallite size is obtained using the Debye-Scherrer formula [35, 39]:

$$D = \frac{0.9\lambda}{\beta \cos(\theta_i)} \quad (7)$$

where D is the crystallite size and β is the FWHM of the Bragg peak in radians. Note that the FWHM should be corrected for the resolution of the instrument. The crystallite size in bulk was calculated using the equation 7 from the width of the Bragg peaks when they are away from the specular condition.

In order to check the alignment of the lamellar sheets with the interface, the reflection was also measured while moving the sample over a small range of angles around the first order Bragg peak. This type of measurement is called a rocking curve where the full width half maximum (FWHM) of the intensity observed at the center of the detector gives an estimate of the alignment of the layers parallel to the interface.

Sample holder

The sample holder for this experiment has been described previously by our group [40]. Briefly, in the set up for this experiment, the sample was sealed with a PTFE gasket between the silicon crystal and a polycarbonate base with injection and outlet ports. The temperature of the cell was controlled using a Julabo bath, circulating water through the aluminum parts that clamp the crystal and the base. The sample was injected into the cell at 20 °C and the measured at 20, 30, 40, 50, 60 °C and again at 20 °C after exposure to the high temperature. This sequence of heating and subsequent cooling can be understood as allowing an observation of the influence of annealing at an elevated temperature. For each temperature rise, a pause of about 10 minutes was performed before data collection. On cooling, a longer interval of 30 minutes was allowed for thermal equilibration of the water circulating bath and sample.

Results and discussion

Figure 2 shows the reflectivity data and the model fits from 55 vol.% Brij L4 at 20 °C (after injecting the sample), on the left, and after heating and then cooling the sample back to 20 °C on the right side. Fitting parameters obtained from the model fits for the sample at different temperatures at both surfaces are presented in Table S1, supporting information. The reflectivity data shows several orders of Bragg peaks, which is an indication of many lamellae aligning themselves parallel to the surface. The sample shows very strong reflection, with the first order Bragg peak reaching more than 10 % of the incident beam intensity, corresponding to a reflectivity >0.1 . A self-organizing sample with such strong scattering provides a good model system to study the effect of different parameters on the distortion of the lamellar structure. Scattering from the sample is so high that it can have the potential to be used as a simple, cheap and readily available liquid neutron monochromator. Modelling the reflectivity data showed that surfactants self-

assemble into multilayer structure with a bilayer thickness of $\sim 58 \text{ \AA}$ aligning with the solid surface. This spacing corresponds to the spacing expected for 55 vol.% Brij L4 in water and suggests that surface structure resembles the bulk. It is interesting to compare the present results with other systems, such as sodium aerosol-OT in water. The lamellar phase forms at low concentrations, about 10%, because of the charge on the ionic groups and it forms multilayer structures at various interfaces [41, 42] at even lower concentrations. The spacing observed even at the lowest concentrations corresponded to 10% surfactant [43]. This has indicated that a surface pre-transition occurred in that system.

At $Q < 0.08 \text{ \AA}^{-1}$ there is a large contribution to the background due to diffraction from the bulk of the sample as mentioned above and this region was excluded from the fits. As expected the observed intensity is larger than the calculated reflectivity because extra intensity is contributed from a distribution of crystallites in the bulk with less-defined orientation.

The same surfactant sample shows different reflectivity at the rough and smooth surfaces. The difference is very clear in the intensity of the first order Bragg peak which showed to be highly influenced by the repetition number of bilayers. At 20 °C (left side of figure 2), the number of the lamellae sheets parallel to the surface at the smooth surface was found to be approximately 100 whereas that for the rough surface is around 30 repetitions. This shows that roughness even smaller than lamellar spacing can disturb the layering and structure of self-assembled lamellae.

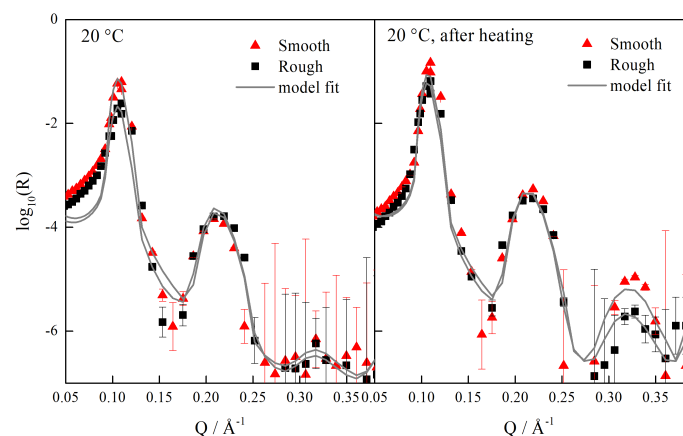


FIG 2. Reflectivity data from Brij L4 against the smooth surface (triangles) and the rough surface (squares) after sample injection at 20 °C on the left, and after heating the sample at 20 °C, on the right side.

The effect of temperature change on the intensity of different order Bragg peak is shown in Figure 3. It is evident that the intensity of peaks increases with temperature for both surfaces but the increase is more pronounced for the sample in contact with the smooth surface (larger gradient). The parameters that describe the fits to the reflectivity curves at the various temperatures are shown in the supporting information (Table S1). The disorder, which is approximated as an average root mean square displacement, increases with temperature but the other changes are small. The number of water molecules per surfactant molecule remains in the range 6 to 8. A significant effect was found to be the increase in the number of layers (N). Our results show that increasing the temperature helps the lamellar structure to order and align particularly for the case of the solid surface. As a result of increasing the temperature, thermal fluctuation in the structure plays an important role in changing the relative intensity between the peaks. The mean displacement of lamellae due to thermal fluctuations obtained from the model fits at each temperature is shown in Figure 4. The amplitude of the thermal fluctuations that are reported in Figure 4 are of the same order as the roughness at the smooth surface. For the rough surface the local static variations in height are significantly larger than the thermal fluctuations and are seen to reduce substantially the orientational alignment. Some further test measurements on a surface with at least 100 Å roughness did not show significant specular scattering but only the diffraction from bulk lamellar phase with poor alignment. The data for the sample did not allow further quantitative evaluation. These results correlate with observations of Imai et al that large spherical particles completely destroy lamellar order in the similar system of C₁₂EO₅/water [19].

The Caillé parameter for the lamellae calculated from equation 6 was found to increase from 0.04 at 20 °C to 0.18 at 60 °C. This can be compared, for example, to a value of 0.08 reported [37] for lipid bilayers formed from DMPC (1,2-dimyristoyl-sn-glycero-3-phosphocholine) at 30 °C. This suggests that the surfactant lamellae have broadly similar elastic moduli to those of saturated phospholipid membranes.

The displacement of the surfactant layers increased as expected with temperature (Loison et al. 2003) in a similar way for Brij against both surfaces. However, when the sample is cooled again to 20 °C, after heating, the displacement for the Brij against

smooth surface is observed to be very small or even negligible. It is smaller than that seen after the initial injection of the sample at 20 °C. An explanation could be that when the sample was injected, part of the structure was dominated by the influence of flow on the orientation. Possibly such alignment could have caused extra fluctuation that remain ‘frozen’ and which could not be distinguished from the thermal fluctuations. While increasing temperature increases the fluctuations, the annealing allows the surfactants to align themselves better with the surface. For the Brij at the rough surface, however, roughness distortion was strong enough to prevent further improvement of the alignment.

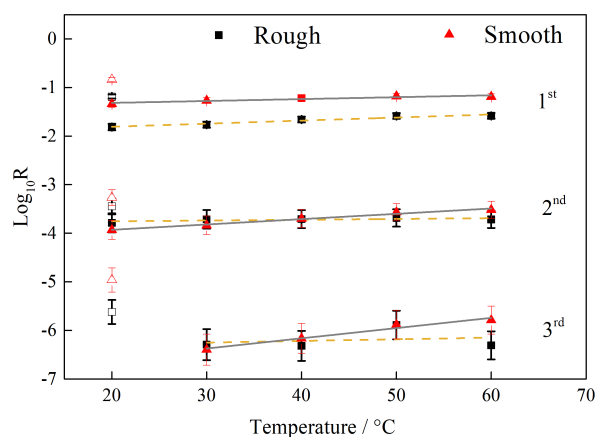


FIG 3. Changes in the absolute reflectivity of the different order Bragg peaks with temperature, for the sample at the smooth surface (triangles) and the rough surface (squares). Open symbols indicate the values for heated sample at 20 °C.

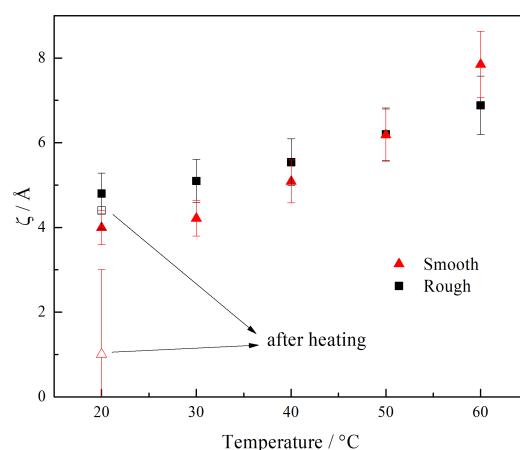


FIG 4. Changes in thermal fluctuations, determined as a Debye-Waller factor, with temperature obtained from modelling reflectivity data for the smooth (triangles) and rough (squares) surfaces. The open symbols indicate the values after heating and then cooling the structure.

One of the evident differences between the reflectivity from the sample at two surfaces was the intensity of the Bragg peaks. Figure 5a and b show the two-dimensional shape of the first order Bragg peaks when the peak is at the specular reflection condition, after heating and then cooling the sample. The sum along the vertical direction for each of the detector image is shown in Figure 5c. The first order Bragg peak from the sample at the rough surface is less intense and more diffuse. The peak has nearly twice the width, which indicates again that layers of surfactant are less well-aligned with the interface. This was consistent with the results obtained from the model fits that there are nearly twice as many layers aligned with the smooth surface at as compared to the rough surface.

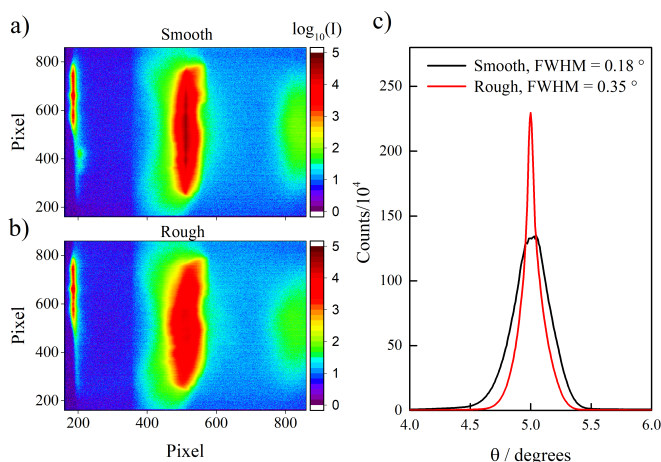


FIG 5. Scattering pattern observed on the two-dimensional detector when the first order Bragg peak is in the specular condition (a and b) and the sum of the intensity in vertical lines down the detector (c) showing the different FWHM.

The lamellar domain size in the bulk was calculated using equation 8 and the results are shown in Figure S8, supporting information. The crystallite size in the bulk for the sample against smooth surface corresponds to about 25 layers whereas that for the rough surface corresponds to about 17 layers. This suggests that the influence of the interface can extend over several layers into the bulk. However, part of the initial alignment and domain size may arise from the flow that occurs on filling the cell. This is likely to be different for the two surfaces. Figure 6 shows rocking scans measured at the highest temperature and after cooling the sample back to 20 °C. There is a significant difference at each temperature between rocking curves measured for the sample against the two surfaces. Rocking scans for the sample is sharper and more intense

when the sample is against the smooth surface, which confirms the results found from the model fits that the lamellar forms a better-aligned structure against the smooth surface.

The intensity of the peaks after heating the sample increased compared to 60 °C for both surfaces. This increase was however more pronounced for the sample at the smooth surface. This shows that annealing effect can improve the alignments at the smooth surface more than that at the rough surface.

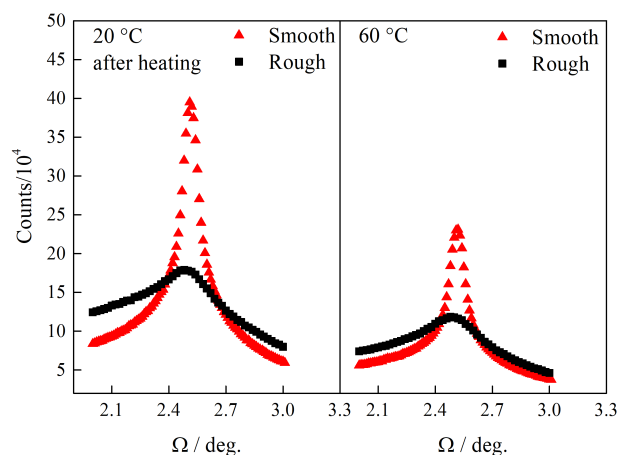


FIG 6. Rocking curves measured on the first-order Bragg peak at the highest temperature and after heating. Ω is the angle of the sample.

The overall description of the structure near the surface and in the bulk, is confirmed by looking at the width of the first order lamellar peak as the sample is scanned in angle. This is shown in Figure 7. The peak is seen on the detector for a range of angles either side of the condition where it is aligned with the specular reflection. On either side of the specular condition the peak is broad. It becomes markedly narrower at the specular reflection. The width can be used to calculate a domain size using Eq. 8 and when allowance is made for the instrumental resolution the size corresponds to about 25 layers for the sample in the bulk contained with the smooth surface and about 17 layers when contained by the rough surface (see Figure S8). At the specular condition, the peak width is much narrower although the effect is more pronounced for the smooth surface. The size corresponds well with the number of layers obtained by directly fitting the reflectivity data in Figure 2 and reported in Table S1. The different domain size found in the bulk is again indicative of the surface or the flow altering the overall structural morphology when the cell is filled.

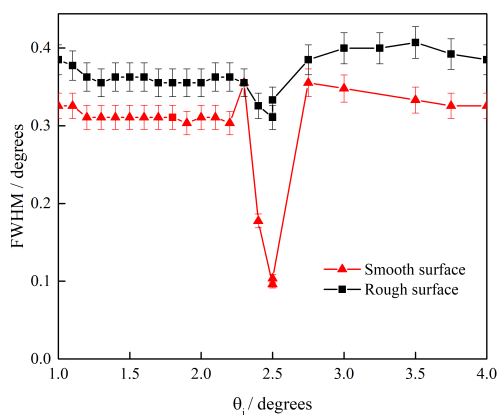


FIG 7. Width of the 1st order diffraction peak for 55 vol.% Brij L4 in D₂O as a function of sample orientation with respect to the incident beam, θ_i . When the diffraction peak is at the specular condition marked narrowing occurs as there are many well-aligned layers at the interface, particularly for the smooth surface.

The effects of surface roughness and the temperature were similar on the intensity and the width of the reflectivity peaks as well as for the rocking curves measured for a sample of 40 vol.% Brij in D₂O against the same smooth and rough surfaces (see Figure S4-S7, supporting information). However, modelling the data and obtaining quantitative values for the fit parameters was more challenging than for the more concentrated system. The lamellar spacing becomes larger and the different order Bragg peaks are close to each other. Hence the effects of overlapping peaks are more pronounced. This means that estimating reflectivity and subtracting the true background from overlapping peaks becomes very challenging.

As previously, the strong Bragg peaks indicate clearly a layered structure. The position of the first order Bragg peak corresponds to a repeat distance of 84 Å for the bilayers. For a dilution from 55 vol.% to 40 vol.% surfactant, the spacing is expected to change from 58 Å to 80 Å. This correspondence is close enough to suggest that the lamellar structure at the interface corresponds to the bulk concentration.

The reflection peak that is shown in Figure 5 is apparently on a background that is part of a Debye-Scherrer ring of diffracted intensity from the bulk that is partially aligned. The slit collimation used in this experiment and the relatively small part of the total scattering that is observable on the two-dimensional detector precludes quantitative

determination of the orientation distribution. The curvature of this background is also apparent in the profiles obtained by summing vertically that are shown in Figure S3 with a tail of higher intensity on the low-angle side of the diffraction peak. The other apparent texture in the observed peaks probably arises from the non-uniform distribution of neutron flux in the guide system of the reflectometer but this spatial variation is not significant in respect of the analysis of integrated intensities that has been described above. A more advanced data analysis that would include these features, might allow further information to be obtained from the background scattering.

Conclusions

The well-aligned multilayer structure formed at a solid/liquid interface allows better determination of Bragg peak intensity than experiments on randomly aligned lamellar aggregates as seen in conventional small-angle neutron scattering such as those of Strey et al [26]. The present study has exploited this advantage to explore the effect of surface roughness and temperature on the alignment of the non-ionic surfactant, C₁₂EO₄, at solid surfaces using neutron reflectometry. The results showed that 55 vol.% C₁₂EO₄ in D₂O self-assembles into multilayer layer structures that extends about a micrometer into the bulk. Such a system provides a model for understanding physics of multilayers. Roughness of the order of the lamellar spacing reduces, but did not completely eliminate, the alignment of the lamellar structure at the interface. At a smooth surface, heating the sample and subsequent cooling back to 20 °C increases the number of aligned bilayers from 100 to 120 layers. For the rough surface this increase was from 30 to 70 layers. In general fluctuations determined from the reflectivity were found to increase as expected with temperature. The reversibility was found to be different for the sample near smooth and rough surfaces, as it is apparent that near the smooth surface some static disorder was present in the initial sample. A possible explanation could be that when the sample was measured at 20 °C immediately after injection, the alignment was influenced by the flow orientation. When the sample is heated, the larger fluctuations can allow the sample to align with the interface.

The major features of the orientation and structure are found also at the lower surfactant concentration of 40 vol.%. This implies that structures tailored with particular lamellar spacings can be obtained

simply by concentration change. It is interesting that very strong diffraction can be obtained from fluid samples reaching more than 0.1 in reflectivity. The width of the Bragg diffraction peak can be modified by simple thermal treatment. This observation suggests that such simple, cheap materials can also offer a new route to develop monochromators for neutrons, or to create other devices that require well-ordered and aligned structures over many centimeters.

References

- J. Yang. *Curr. Opin. Colloid. Interface Sci.* 7, 276-281 (2002).
- C. Prieto and L. Calvo, *J. App. Chem.*, 930356 (2013).
- E. Ha, W. Wang, J. Y. Wang, *J. Pharm. Sci.*, 91, 2252-2264 (2002).
- B. A. Kerwin, *J. Pharm. Sci.*, 97, 2924-2935 (2008)
- J. Penfold, I. Tucker, and R. K. Thomas, *Langmuir*, 21, 6330-6336 (2005).
- G. D. Parfitt and C. H. Rochester, *Adsorption from Solution at the Solid/Liquid Interface*, Academic Press London; New York (1983).
- J. N. Israelachvili, *Intermolecular and Surface Forces*, Academic, (2008).
- R. Nagarajan, *Langmuir*, 18, 31-38 (2001).
- G. T. Pickett, T. A. Witten, and S. R. Nagel, *Macromolecules*, 26, 3194-3199 (1993).
- Z. G. Workineh and A.G. Vanakaras, *Polymers*, 6, 2082-2099 (2014).
- M. I. Boamfa, M. W. Kim, J. C. Maan, and Th. Rasing, *Nature*, 421, 149-152 (2003).
- M. C. Gerstenberg, J. S. Pedersen, and G. S. Smith, *Phys. Rev. E* 58, 8028 (1998).
- N. A. Lockwood, J. K. Gupta, and N. L. Abbott, *Surface Science Reports*, 63, 255-293 (2008).
- L. S. Hirst and G. Charras, *Nature*, 544, 164-165 (2017).
- L. Ginsberg, J. R. Atack, S. I. Rapoport, and N. L. Gershfeld, *Molecular and Chemical Neuropathology*, 19, 37-46 (1993).
- S. Jeong, J. Y. Kim, B. H. Kim, H. Moon, and S. O. Kim, *Materials Today*, 16, 468-47 (2013).
- V. Kapaklis, S. Grammatikopoulos, R. Sordan, A. Miranda, F. Traversi, H. von Kanei, D. Trachylis, P. Pouloupoulos and C. Politis, *Journal of Nanoscience and Nanotechnology*, 10, 6056-6061 (2010).
- M. Imai, R. Mawatari, K. Nakaya, and S. Komura, *Eur. Phys. J. E* 13, (2004), 391-400.
- M. Imai, Y. Suganuma, K. Nakaya, and S. Komura, *J. Phys.: Condens. Matter*, 17, S2929-S2935 (2005).
- Y. Suganuma, N. Urakami, R. Mawatari, S. Komura, K. Nakaya-Yaegashi, and M. Imai, *The Journal of Chemical Physics*, 129, 134903 (2008).
- A. P. Dabkowska, C. S. Niman, G. Piret, H. Persson, H. P. Wacklin, H. Linke, C. N. Prinz, and T. Nylander, *Nano Letters*, 14, 4286-4292 (2014).
- S. Wu, L. Shi, L. B. Garfield, R. F. Tabor, A. Striolo, and B. P. Grady, *Langmuir*, 21, 6091-6098 (2011).
- G. Fragneto, R. K. Thomas, A. R. Rennie, and J. Penfold, *Langmuir*, 12, 6036-6043 (1996).
- D. J. Mitchell, G. J. T. Tiddy, L. Waring, T. Bostock, and M. P. McDonald. *J. Chem. Soc., Faraday Trans. I* ,79, 975-1000 (1983).
- P. G. Nilsson, H. Wennerström, and B. Lindman, *J. Phys. Chem.*, 87, 1377-1385 (1983).
- R. Strey, R. Schomäcker, D. Roux, F. Nallet, and U. Olsson, *J. Chem. Soc. Faraday Trans.*, 86, 2253-2261 (1990).
- S. Nouhi, M. S. Hellsing, V. Kapaklis, and A. R. Rennie, *Journal of Applied Crystallography*, 50, 1066-1074 (2017).
- S. Mattauch, A. Koutsioubas, and S. Pütter, *Journal of large-scale research facilities JLSRF*, 1, A8 (2015).
- S. Mattauch, A. Koutsioubas, U. Rücker, D. Korolkov, V. Fracassi, J. Daemen, R. Schmitz, K. Bussmann, F. Suxdorf, M. Wagener, P. Kämmerling, H. Kleines, L. Fleischhauer-Fuß, M. Bednareck, V. Ossoviy, A. Nebel, P. Stronciwilk, S. Staringer, M. Gödel, A. Richter, H. Kusche, T. Kohnke, A. Ioffe, E. Babcock, Z. Salhi, and T. Bruckel, *J. Appl. Cryst.* 51, 646-654 (2018).
- F. Abelès, *Ann. Phys.* 1950, 11, 307-309 & 310314.
- A. R. Rennie, *Neutron Reflection and Neutron Reflectometers, Analysis Programs*, (2018): <http://www.reflectometry.net/reflect.htm#Analysis>
- M. S. Hellsing, A. V. Hughes, and A. R. Rennie, *Langmuir*, 27, 4669-4678 (2011).
- L. Nénot and P. Croce, *Rev. Phys. Appl.*, 15, 761-779 (1980).
- G. L. Squires, *Introduction to Thermal Neutron Scattering*, Dover: Mineola, NY, (1996).
- B. E. Warren *X-Ray Diffraction*. Addison-Wesley, Reading, MA. (1969).
- A. Caillé, *C.R. Acad. Sci. Paris Série B*, 274, 891-893 (1972).
- J. F. Nagle and S. Tristram-Nagle, *Biochimica et Biophysica Acta (BBA) - Reviews on Biomembranes*, 1469, 169-195 (2000).
- K. Nag (edt.), *Structure and Dynamics of Membranous Interfaces*. John Wiley & Sons, Hoboken (NJ), 45-81 (2008). M. Rappolt and G. Pabst, Chapter 3: Flexibility and Structure of Fluid Bilayer Interfaces.
- S. J. S. Qazi, A. R. Rennie, J. K. Cockcroft, and M. Vickers, *Journal of Colloid and Interface Science*, 338, 105-110 (2009).
- A. R. Rennie, M. S. Hellsing, E. Lindholm, and A. Olsson, *Rev. Sci. Inst.* 86, 016115 (2015).
- Z. X. Li, A. Weller, R. K. Thomas, A. R. Rennie, J. R. P. Webster, J. Penfold, R. K. Heenan, and R. Cubitt, *Journal of Physical Chemistry B*, 103, 10800-10806 (1999).
- Z. X. Li, J. R. Lu, R. K. Thomas, A. Weller, J. Penfold, J. R. P. Webster, D. S. Sivia, and A. R. Rennie, *Langmuir*, 17, 5858-5864 (2001).
- C. Loison, M. Mareschal, K. Kremer, and F. Schmid, *The Journal of Chemical Physics*, 119, 13138-13148 (2003).